Chapter

4

PET imaging of glucose metabolism, neuroinflammation and demyelination in the lysolecithin rat model for multiple sclerosis

Daniele de Paula Faria, Erik F.J. de Vries, Jurgen W.A. Sijbesma, Carlos A. Buchpiguel, Rudi A.J.O. Dierckx, Sjef C.V.M. Copray

Submitted

ABSTRACT

Injection of lysolecithin in the central nervous system results in demyelination accompanied by local activation of microglia and recruitment of monocytes. PET imaging, using specific tracers, may be an adequate technique to monitor these events in-vivo and therefore may become a tool for monitoring disease progression in MS patients. In this study, we aimed to evaluate the potential of PET imaging in monitoring local lesions, using [^{11}C]MeDAS, [^{11}C]PK11195 and [^{18}F]FDG as PET tracers for myelin density, microglia activation and glucose metabolism, respectively. Sprague-Dawley rats were stereotactically injected with either 1% lysolecithin or saline in the corpus callosum and striatum of the right brain hemisphere. PET imaging was performed 3 days, 1 and 4 weeks after injection. Animals were terminated after PET imaging and the brains were explanted for (immuno)histochemical analysis. PET imaging was able to detect local demyelination induced by lysolecithin in the corpus callosum and striatum with [^{11}C]MeDAS and concomitant microglia activation and monocyte recruitment with [^{11}C]PK11195. [^{18}F]FDG imaging demonstrated that glucose metabolism was maintained in the demyelinated lesions. In conclusion, PET imaging with multiple tracers allows simultaneous in-vivo monitoring of myelin density, neuroinflammation and brain metabolism in small MS-like lesions, indicating its potential to monitor disease progression in MS patients.

INTRODUCTION

Research on pathogenic processes in multiple sclerosis (MS) notably depends on animal models for this disease. Local disintegration of myelin by injection of lysolecithin in the central nervous system (CNS) has been used in mouse, rat, rabbit, cat and monkey to generate models for MS (Blakemore and Franklin, 2008; Dousset et al, 1995; Gensert and Goldman 1997; Hall, 1972; Triarhou and Herndon 1986; Waxman et al 1979; Woodruff and Flanklin, 1999). Lysolecithin-induced demyelination is accompanied by recruitment of microglia activation and monocytes that remove myelin debris, mimicking similar processes occurring in MS. Since lysolecithin has a short biological half-life (5 hours), damage is restricted in time and space, allowing local oligodendrocyte precursor cells to completely restore the myelin sheaths.

Most studies in MS models rely on *ex vivo* analysis of brain tissue or on structural imaging. Magnetic Resonance Imaging (MRI) is currently the standard imaging tool in MS. However, detection of MS lesions by MRI is not very specific, as it is based on changes in water content, rather than on specific disease-related processes (Fillip and Rocca, 2011). Functional imaging, on the other hand, may provide more disease-specific and quantitative information. In particular, Positron Emission Tomography (PET) shows potential to become a valuable imaging tool for monitoring MS-related biological processes over time, such as brain metabolism, myelin content and neuroinflammation in focal lesions in the CNS.

[^{11}C]MeDAS is a recently published PET tracer for imaging myelin content (Wu et al, 2010). This tracer has a stilbene based structure, related to the congo red dye (Stankoff et al, 2006), and has been shown to be able to detect differences in myelin content in the brain between wild-type and hyper-myelinated mice (Wu et

al, 2010) and could also reveal demyelinated lesions in the spinal cord of lysolecithin and EAE rat models (Wu et al, 2013). [^{11}C]PK11195 is a PET tracer for imaging 18 kDa translocator protein (TSPO), which is expressed in all glial cells, and over-expressed during neuroinflammatory process (Doorduin et al, 2008). PET imaging with this tracer can therefore provide a noninvasive measure of the activation status of microglia and monocytes, although signal from reactive astrocytes can also occur. [^{18}F]FDG is a radiolabeled glucose analogue that is widely used as a PET tracer to measure glucose metabolism. [^{18}F]FDG PET images show increased uptake in tissues with metabolically active cells, like growing tumors, or in organs that rely on glucose as a source of energy, like the brain (Chierichetti and Pizzolato, 2010; Kang et al, 2012). [^{18}F]FDG uptake in brain tissue is generally considered as a surrogate biomarker of brain activity.

In this study, we aimed to assess the feasibility of in-vivo monitoring of MS-specific disease processes with PET. To this purpose, we used a combination of three PET ligands to monitor demyelination, remyelination, glucose metabolism and neuroinflammation in small MS-like brain lesions in the lysolecithin rat model.

METHODS

Animals

Demyelination was induced in 8-10 weeks old male Sprague-Dawley rats (Harlan, the Netherlands) by stereotactic injection of 1% lysolecithin (lysophosphatidyl choline, LPC; Sigma-Aldrich) in saline, in the corpus callosum and striatum on the right-hand side of the brain (stereotactic coordinates: anterior -0.30, lateral -3.0 and ventral -3.0, -4.2, -5.0 mm to the Bregma point). Control animals were injected with saline. Food and water were given *ad libitum* and the animals were daily monitored for body weight and mobility.

Animal experiments were performed according to the Dutch Regulations for Animal Welfare. The protocol was approved by the Institutional Animal Care and Use Committee of the University of Groningen (protocol: DEC 5040J).

PET tracers

[^{18}F]FDG, [^{11}C]-(*R*)-PK11195 and [^{11}C]MeDAS were produced as previously described (Wu et al, 2010; Cremer et al, 1992). Radiochemical purity was always >95%.

PET imaging

[^{18}F]FDG (n=4) and [^{11}C]PK11195 (n=6) PET imaging was performed on experimental animals 3 days, 1 and 4 weeks after injection of 1% lysolecithin (Figure 1). Control animals were scanned at 3 days and 1 week after injection of saline. [^{11}C]MeDAS PET (n=6) was performed at 1 week and 4 weeks time points. Animals were anesthetized with 2% isoflurane in medical air. Before [^{18}F]FDG PET, blood glucose levels were determined by taking a drop of blood from the tail vein (one touch ultra 2 glucose meter, Johnson & Johnson). The animals were either intraperitoneally injected with 20-30 MBq of [^{18}F]FDG, or intravenously injected in the penile vein with 50-60 MBq of [^{11}C]PK11195 (specific activity >30 GBq/µmol) or 50-60 MBq of [^{11}C]MeDAS (specific activity >50 GBq/µmol). Animals were allowed to wake up in their home cage after administration of [^{18}F]FDG or [^{11}C]PK11195 for better tracer distribution. After 40 min, these animals were anesthetized again and placed in the PET camera (Focus 220, Siemens; spatial resolution 1.35 mm at the center of the field-of-view). Acquisition of a 30-min static emission scan was started 45 minutes after tracer injection. [^{11}C]MeDAS PET was performed by a 60-min dynamic acquisition, starting immediately after tracer

injection. After the emission scan, a transmission scan of 515 seconds with a ^{57}Co point source was performed for attenuation and scatter correction.

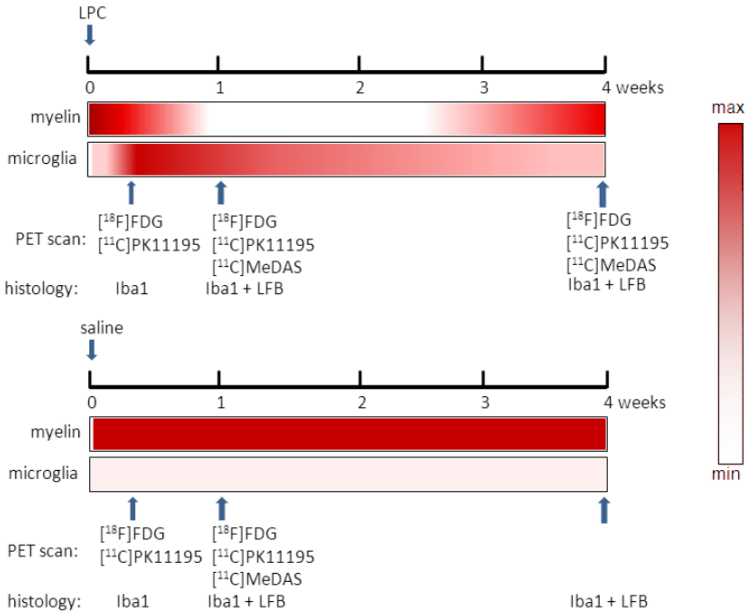

Figure 1: Scheme representing the study design and the time points of analyses after LPC or saline injection in the corpus callosum/striatum. The (intensity of the) red color in the bars reflects the state of myelination or microglia activation level at the site of injection.

PET image reconstruction and analysis

Emission sinograms were iteratively reconstructed (OSEM2d, 4 iterations) after being normalized, corrected for attenuation and decay of radioactivity. The [^{11}C]MeDAS list-mode data was separated into 20 frames (8x30, 2x60, 2x120, 2x150, 3x300 and 3x600 sec). After reviewing the time-activity curves, [^{11}C]MeDAS uptake was quantified for the last 30 min of the scan by summation of the last 3 frames. Static [^{18}F]FDG and [^{11}C]PK11195 were reconstructed as a single 30-min frame.

The images were analyzed by INVEON software (Siemens). PET images were manually co-registered with a rat brain T2 MRI template available in the software. Regions of interest (ROI) were drawn for focal lesion (injection site), contralateral side, left and right brain hemisphere and whole brain on the MRI template and copied to the [^{18}F]FDG, [^{11}C]PK11195 and [^{11}C]MeDAS PET images. For each ROI, the radioactivity concentration was determined and corrected for the injected dose and body weight to give Standardized Uptake Values (SUV). [^{18}F]FDG brain uptake was normalized for the blood glucose level (5.55 mmol/L; Woo et al, 2008) at the time of tracer injection: SUV_{corr}= [(SUV x blood glucose (mmol/L)) / 5.55 mmol/L].

For localizing the portion of corpus callosum and striatum affected by the injection and drawing the ROI "lesion" in the PET image, Luxol Fast Blue histochemistry of each respective animal was used as a visual guide. The ROI of the lesion was copied to the contralateral side for quantification of tracer uptake in the same region of the unaffected hemisphere. For [^{11}C]MeDAS the results are presented as lesion-to-contralateral ratios.

In vitro autoradiography

The distribution of [^{11}C]MeDAS binding in the rat brain was also analyzed by *in vitro* autoradiography. Brain cryosections (20 μm) of the demyelination group (1 week after lysolecithin injection) and the control group (1 week after saline injection) were incubated in [^{11}C]MeDAS solution (30-40 MBq in 40-50 ml PBS) for 10 minutes and washed in running tap water for 20 minutes. After drying by exposure to air for 15 min, the sections were exposed to a multisensitive phosphor storage screen for 2 hours. The exposed phosphor screens were scanned with a Cyclone® phosphor system (PerkinElmer) and images were analyzed by Optiquant software.

(Immuno)histochemistry analysis

Changes in the level of myelination were detected by Luxol Fast Blue histochemistry (all animals). Iba1 immunohistochemistry was used for detection of microglia activation and monocyte invasion in the animals submitted to [^{11}C]PK11195 PET (3 animals for the 3 days time point and 6 animals for the 1 week and 4 weeks time points). Protocols are published elsewhere (Olah et al, 2012).

Statistical analysis

The results are presented as mean ± standard deviation. The data passed the Kolmogorov-Smirnov test for normality and the Bartlett´s test for common variance. Differences between groups were analyzed for statistical significance by 2-way ANOVA (GraphPad Prism) using a Bonferroni post hoc test. Differences were considered significant when $p < 0.05$.

RESULTS

Induction of lysolecithin lesions

The size of the demyelinated lesion appeared to depend on the volume as well as the speed of lysolecithin injection. Injection of only 3 μl 1% lysolecithin at a speed of 1 μl/min in the corpus callosum resulted in only minute lesions (< 1 mm), not detectable with PET. On the other hand, injection of 7 μl 1% lysolecithin, divided in 3 μl in corpus callosum and 2x2 μl in striatum at a speed of 1 μl/min resulted in massive tissue damage and necrosis, still visible 4 weeks after injection (Figure 2A).

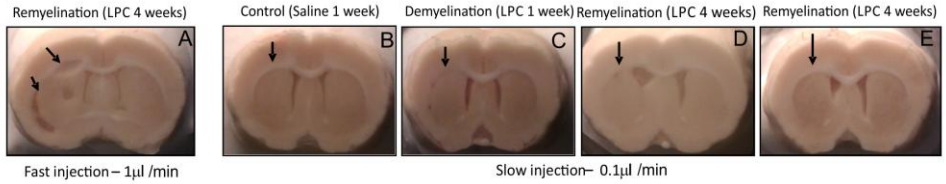

Figure 2: Coronal view of rat brains after stereotactic injection of 1% lysolecithin (A,C,D,E) or saline (B). Four weeks after fast injection of lysolecithin (1 μl/min) substantial tissue damage (arrows) is induced (A). Slow speed (0.1 μl/min) saline injection does not lead to tissue damage or demyelination at the injection site (arrow) at one week after injection (B). Slow (0.1 μl/min) 1% lysolecithin injection results in demyelination in the right corpus callosum (arrow) after one week (C) and partial remyelination (arrow) without tissue damage (D), or complete remyelination (arrow) without tissue damage (E) after 4 weeks.

However, injection of 7 μl of 1% lysolecithin at the same coordinates, but at a speed of only 0.1 μl/min, resulted in small, reproducible demyelinated lesions (1.5 - 2 mm) without nonspecific tissue damage after 1 week (Figure 2C). Control injections with 7 μl saline at the same speed did not induce significant lesions (Figure 2B). Four weeks after slow injection of lysolecithin the remyelination rate was variable (Figure 2D-E). Animals did not present any symptoms or adverse effects (weight loss or mobility disturbance) after slow saline or 7 μl 1% lysolecithin injection.

[^{18}F]FDG PET imaging of glucose metabolism

[^{18}F]FDG PET imaging confirmed the absence of tissue necrosis after 7μl 1% lysolecithin injection at a speed of only 0.1 μl/min (Figure 3). No significant differences were found in blood glucose-corrected [^{18}F]FDG uptake in the injected site (lesion) between animals injected with saline and lysolecithin for any time point (SUV_{corr} 4.0±1.1 and 3.1±0.6 for controls at 3 days and 1 week after saline

injection vs. 4.0±1.5, 3.1±0.4 and 3.9±1.1 for experimental animals at 3 days, 1 and 4 weeks after injection of lysolecithin, respectively). Contralateral side and whole brain did not show significant differences either.

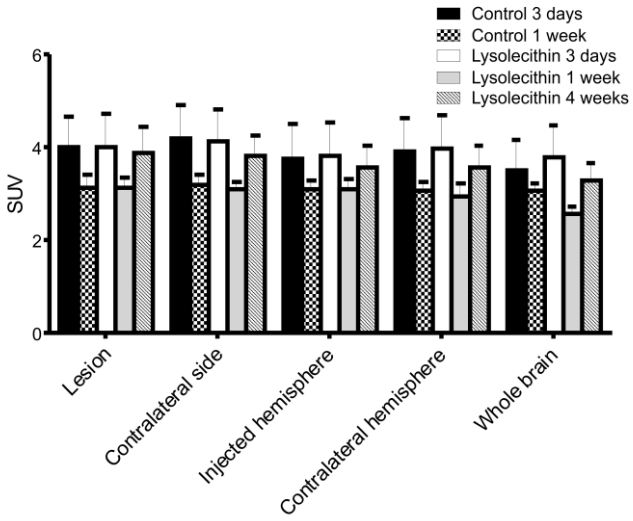

Figure 3: [^{18}F]FDG uptake in different brain regions of the control group and the lysolecithin group at different time points (3 days, 1 week and 4 weeks) after stereotactic injection.

[^{11}C]PK11195 PET imaging of neuroinflammation

Microglia activation and monocyte recruitment, induced by the injection of lysolecithin or saline, were evaluated by [^{11}C]PK11195 PET imaging. *In-vivo* PET images (Figure 4) show focal inflammation at the injection site in all animals 3 days after lysolecithin injection, but not in animals injected with saline. At day 7 after lysolecithin injection, [^{11}C]PK11195 uptake was still increased at the injection site. Four weeks after lysolecithin injection, however, none of the animals showed

visible [^{11}C]PK11195 uptake at the injection site, suggesting that neuroinflammation had completely resolved.

Quantitative analysis of the [^{11}C]PK11195 PET data revealed a significantly higher tracer uptake ($p<0.001$) in the lesion of lysolecithin-treated (0.79±0.07) rats at day 3 after injection, as compared to controls (0.43±0.11) (Figure 5). After 1 week, the uptake in the lesion was still significantly higher ($p<0.01$) in the lysolecithin group (0.66±0.14) as compared to saline 1 week (0.48±0.07) and significantly decreased ($p<0.05$) as compared to day 3 of lysolecithin injected animals. Tracer uptake was reduced to almost baseline levels (0.55±0.16) after 4 weeks. No significant differences between groups were found in the contralateral side and whole brain.

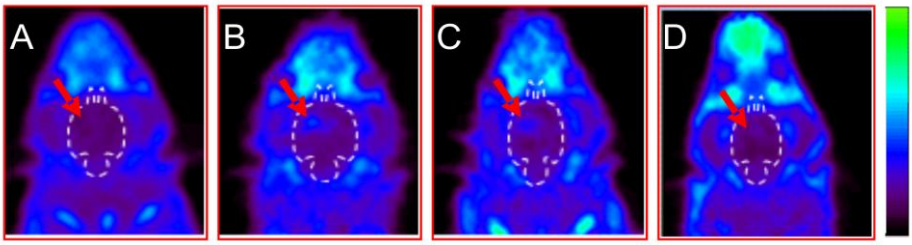

Figure 4: [^{11}C]PK11195 PET images showing coronal sections of the rat heads. Brains are delineated by white interrupted lines and the red arrows show the injection site: (A) 3 days after stereotactic injection of saline; (B) 3 days after stereotactic injection of lysolecithin; (C) 1 week after stereotactic injection of lysolecithin and (D) 4 weeks after stereotactic injection of lysolecithin.

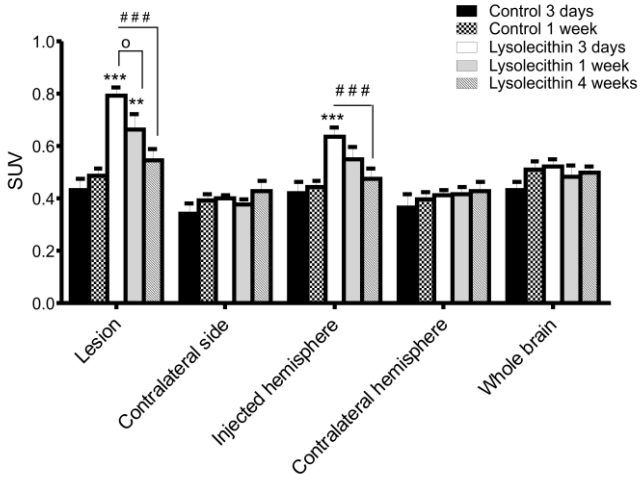

Figure 5: Quantitative [^{11}C]PK11195 uptake in different brain regions of the control animals and the lysolecithin treated rats at different time points (3 days, 1 week and 4 weeks) after stereotactic injection. Significant differences compared to control are indicated by ** ($p<0.01$) and *** ($p<0.001$). Significant differences of the lysolecithin injected animals at day 3 and 1 week is represented by o ($p<0.05$). Significant differences of the lysolecithin injected animals at day 3 and 4 weeks is represented by ### ($p<0.001$).

Immunohistochemical analysis of activated microglia and monocytes

Brain tissue sections were analyzed by immunohistochemistry for activated microglia and monocytes using anti-Iba1 antibodies (Figure 6). In lysolecithin-injected rats, activated microglia was observed in the ipsilateral striatum and corpus callosum at day 3 and 1 week after lysolecithin injection. At week 4, Iba1 staining was strongly reduced, although especially in the striatum it was still higher than in saline-treated animals. No microglia activation was seen in the hemisphere contralateral to the lysolecithin or the saline injection site.

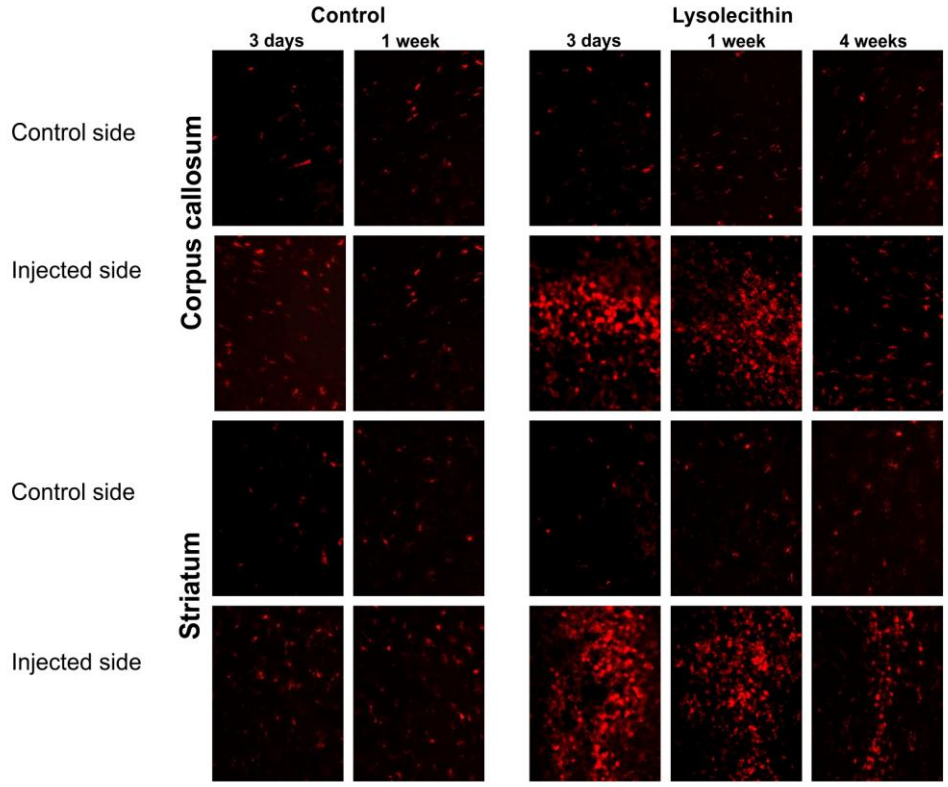

Figure 6: Iba1 immunohistochemistry showing microglia activation and monocyte invasion in the saline and lysolecithin treated rats at different time points after unilateral stereotactic injection in corpus callosum and striatum.

[^{11}C]MeDAS PET imaging of myelin content

Focal demyelination and remyelination in the lysolecithin-induced lesions were evaluated by *in-vivo* [^{11}C]MeDAS PET imaging. [^{11}C]MeDAS PET images (Figure 7) did not show any lesions after saline injection, but clearly delineated the demyelinated lesion as a cold spot 1 week after lysolecithin injection. Four weeks after lysolecithin injection, a focal lesion could still be seen in the PET images.

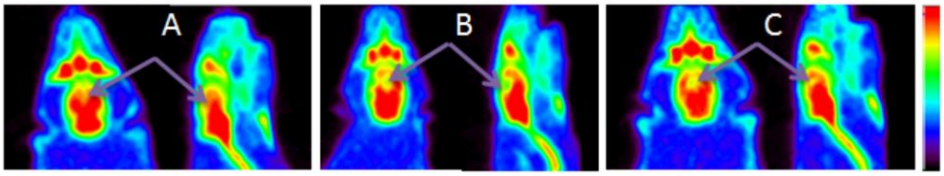

Figure 7: [^{11}C]MeDAS PET imaging showing coronal (left) and sagittal (right) view of the rat heads. (A) No visual lesion 1 week after saline injection; (B) Lesion 1 week after lysolecithin injection; (C) Lesion 4 weeks after lysolecithin injection. Arrows indicate the injection site. Note that the spinal cord is clearly visible in the PET images.

[^{11}C]MeDAS brain uptake showed more affinity to white matter (+40%) then grey matter. Time activities curves (TAC) showed fast washout, with a half-life of 18 minutes. TACs did not show any significant differences between groups for any brain region. The TAC of the injection site (lesion) is represented in figure 8. [^{11}C]MeDAS uptake values (SUV) showed relatively high inter-individual variability between animals (about 12%, 25% and 29% for the control, demyelination and remyelination groups, respectively). Therefore, [^{11}C]MeDAS uptake was quantified as lesion-to-contralateral side ratio. As shown in Figure 8, the [^{11}C]MeDAS uptake ratio was significantly lower in the lysolecithin than in the control group (0.97±0.005), both 1 week (0.90±0.03, $p<0.001$) and 4 weeks after injection (0.91±0.06, $p<0.001$). These results suggest that remyelination was still incomplete 4 weeks after lysolecithin injection. The left -to-right-hemisphere ratio (total brain) did not reveal any significant differences between groups, proving the focal aspect of the lesion.

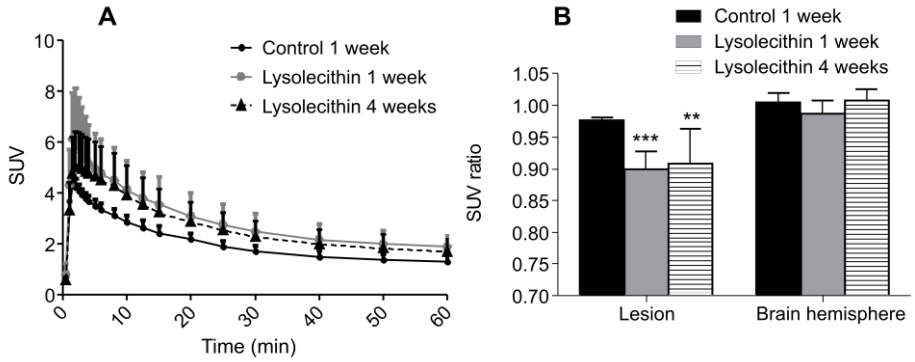

Figure 8: [^{11}C]MeDAS PET uptake quantification. (A) [^{11}C]MeDAS time activity curves of the injected site (lesion) do not show significant differences between groups; (B) [^{11}C]MeDAS lesion-to-contralateral side uptake ratio of the control group, demyelination group (lysolecithin 1 week) and remyelination group (lysolecithin 4 weeks) for lesion site and total brain hemisphere regions-of-interest. Significant differences, as compared to control, are illustrated by *** ($p<0.001$) and **($p<0.01$).

[^{11}C]MeDAS autoradiography

Because the limited spatial resolution of the PET camera (1.35 mm) precludes visualization of the corpus callosum as an individual brain region, [^{11}C]MeDAS binding was assessed by *in-vitro* autoradiography to gain more insight in the spatial distribution and thus the myelin-specificity of this tracer. [^{11}C]MeDAS autoradiography images showed highest tracer uptake in corpus callosum, a brain region with a high myelin density. Saline-injected animals revealed homogeneous uptake in the entire corpus callosum (Figure 9A). In contrast, [^{11}C]MeDAS binding was strongly decreased in the corpus callosum at the site where lysolecithin was injected (lesion/contralateral ratio 0.43), suggestive for demyelination of this part of the corpus callosum (Figure 9B).

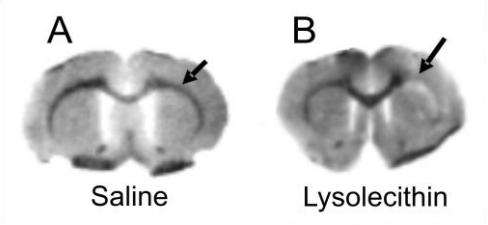

Figure 9: [^{11}C]MeDAS *in vitro* autoradiography showing brain sections 1 week after stereotactic injection of (A) saline and (B) lysolecithin. Arrows indicate the injection site.

Myelin histochemistry

To confirm the results of the [^{11}C]MeDAS PET and autoradiography experiments, Luxol Fast Blue histochemistry for myelin was performed (Figure 10). No myelin damage could be seen after injection of saline, nor was any loss of myelin fibers observed in the contralateral hemisphere of lysolecithin-injected animals. In contrast, focal demyelination in the corpus callosum and striatum was evident at the injection site 1 week after lysolecithin injection. Four weeks after lysolecithin injection, complete remyelination was observed in only 1 animal, partial remyelination was observed in 1 animal, whereas the other 4 animals showed no sign of remyelination.

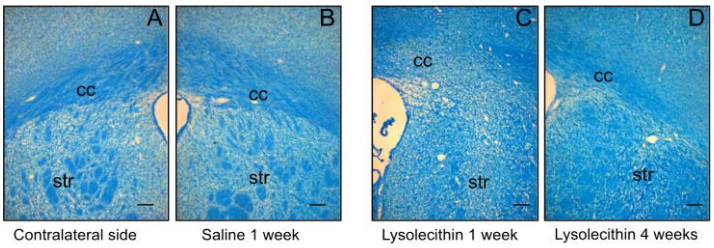

Figure 10: Luxol fast blue staining showing the injection sites in corpus callosum (cc) and striatum (str): (A) contralateral side of the stereotactic injection; (B) injection site 1 week after saline injection; (C) injection site 1 week after lysolecithin injection; (D) injection site 4 weeks after lysolecithin injection. Scale bar = 100 μm.

DISCUSSION

For our small animal PET imaging study, the lysolecithin-induced demyelination lesions needed to be bigger than the resolution of the scanner (1.35mm). However, inducing too large lesions with lysolecithin can lead to nonspecific cellular damage and local necrosis, preventing spontaneous remyelination (Woodruff and Franklin, 1999). Apparently, slow injection of the toxin was crucial for controlled focal demyelination. Lysolecithin diffuses into the white fibers (Waxman et al, 1979) and only a slow steady injection allows the solution to diffuse uniformly, preventing accumulation of a high toxic concentration causing tissue necrosis (Dousset et al 1995; Hall, 1972; Waxman et al, 1979). By standardizing our procedure for the induction of small reversible lesions, we were able to systematically evaluate their characteristics by multiple tracer *in-vivo* PET imaging.

No significant differences in [^{18}F]FDG uptake were detected in our study; in contrast, increased [^{18}F]FDG uptake in inflammatory lesions has been demonstrated in the spinal cord of experimental autoimmune encephalomyelitis model (Radu et al, 2007; Buck et al 2012). Buck et al (2012) were able to detect inflammatory lesions in the spinal cord, but they also demonstrated that [^{18}F]FDG PET presented a low sensibility in detecting inflammatory lesions in the brain. The high physiologic uptake of [^{18}F]FDG in the brain is likely the reason for not detecting inflammatory lesions in this study. The absence of significant local decreases in [^{18}F]FDG uptake after lysolecithin injection seems to indicate that no severe tissue necrosis was induced by our injection procedure.

Based on the previously described time course of lesion formation and recovery (Dousset et al, 1995; Hall, 1972; Hall and Gresgon, 1971; Gegaonkar et al, 2002;

2005), we have chosen to monitor neuroinflammation with [^{11}C]PK11195 PET at 3 days, 1 and 4 weeks after lysolecithin injection. [^{11}C]PK11195 PET, in contrast to [^{18}F]FDG PET, showed the highest uptake at day 3 and uptake was still elevated 1 week after injection. [^{11}C]PK11195 uptake almost returned to baseline levels at 4 weeks after injection. This uptake pattern at the lesion site correlated well with immunohistochemistry of activated microglia and infiltrating monocytes in the same animals.

The demyelination and remyelination processes were monitored at 1 and 4 weeks after lysolecithin injection using [^{11}C]MeDAS. This tracer binds to intact myelin sheaths and its brain uptake is decreased in case of myelin loss (Wu et al, 2010; Wu et al, 2013; Wu et al, 2006). [^{11}C]MeDAS TACs show a faster tracer washout, in agreement with previously published data (Wu et al, 2010) and did not show significant differences between groups due to inter-subject variability, even in normal brain tissue. It is not clear whether the inter-individual variability in [^{11}C]MeDAS uptake is due to individual differences in myelin density in normal brain, to differences in the size of the demyelinated lesion or to differences in tracer delivery to the brain. To overcome inter-subject variability, we used the ratio between tracer uptake at the injection site and at the same region in the contralateral hemisphere (internal control) as a measure for focal demyelination. In this manner, [^{11}C]MeDAS PET was able to show the decrease in myelin content in the focal lesion at 1 week after lysolecithin injection. Despite ongoing remyelination, reduced [^{11}C]MeDAS uptake was still observed in week 4. Histochemistry confirmed that demyelinated lesions were still present in most of the animals 4 weeks after lysolecithin injection.

In absolute terms, the reduction in [^{11}C]MeDAS uptake at the lesion site is lower than expected based on histochemistry. Because the size of the lesion is in the

same range as the spatial resolution of the PET camera, the tracer uptake at the lesion site will be affected by partial volume effects: i.e. the observed signal of the lesion is contaminated with signal from surrounding tissue. Consequently, the measured reduction in tracer uptake at the lesion site will be an underestimation of the actual reduction in tracer uptake, since the surrounding normal brain shows higher tracer uptake than the lesion. *In-vitro* autoradiography indeed confirmed that the reduction of [^{11}C]MeDAS binding in the demyelinated area in the corpus callosum was much larger than the reduction observed by PET imaging, suggesting that the sensitivity of the tracer could be better for larger lesions that are less prone to partial volume effects. Since spill-over is dependent on the lesion size and modern clinical PET cameras can obtain a reconstructed spatial resolution of about 2 mm, the influence of partial volume effects and spill-over is expected to be much smaller in MS patients that generally have larger lesions relative to the spatial resolution of the PET camera.

MRI clearly lacks sufficient specificity to evaluate key cellular processes in MS lesion formation, like microglia activation, monocyte infiltration, demyelination and cell death (Rovira and León, 2008; Szymanski et al, 2010). Our results indicate that PET imaging can monitor cellular processes in lesions over time and thus may be a tool to distinguish between chronic and acute lesions in MS patients. Acute lesions, formed during relapses in relapsing-remitting MS, are characterized by inflammatory infiltrates and active demyelination, processes that can be identified by a local increase in [^{11}C]PK11195 uptake and a decrease in [^{11}C]MeDAS uptake, respectively. Chronic lesions, in the more progressive stages of MS, are characterized by low inflammation and extensive demyelination, possibly accompanied by axonal loss (Constantinescu et al, 2011). Lesions showing low [^{18}F]FDG uptake (low glucose metabolism) and decreased [^{11}C]MeDAS uptake (myelin content loss) may suggest irreversible focal demyelination, while normal

[^{18}F]FDG uptake with decreased [^{11}C]MeDAS uptake may indicate a reversible demyelination or even an ongoing remyelination process.

The specific information about the characteristics of each lesion that is provided by a multiple tracer PET imaging approach can offer most valuable support to the treatment of MS patients and help to assess the effects and mechanisms of new MS drugs.

AKNOWLEDGEMENTS

We would like to thank the Dutch MS Research Foundation (project 10-0700 MS) for financial support and Lian Boerma for the assistance during stereotactic injections and PET scanning.

REFERENCES

Blakemore WF and Franklin RJM. Remyelination in experimental models of toxin-induced demyelination. *Curr Top Microbiol Immunol* 2008; 318:193-212.

Buck D, Förschler A, Lapa C, Schuster T, Vollmar P, Korn T, Nessler S, Stadelmann C, Drzezga A, Buck AK, Wester HJ, Zimmer C, Krause BJ, Hemmer B (2012). 18F-FDG PET detects inflammatory infiltrates in spinal cord experimental autoimmune encephalomyelitis lesions. J Nucl Med 53:1269-76.

Chierichetti F and Pizzolato G. ^{18}F-FDG-PET/CT. *Q J Nucl Med Mol Imaging* 2012. 56:138-150.

Constantinescu CS, Farooqi N, O'Brien K, et al. Experimental autoimmune encephalomyelitis (EAE) as a model for multiple sclerosis (MS). *Br J Pharmacol* 2011. 164:1079–1106.

Cremer JE, Hume SP, Cullen BM, et al. The distribution of radioactivity in brains of rats given [N-methyl-^{11}C]PK11195 *in vivo* after induction of a cortical ischaemic lesion. Nucl Med Biol 1992. 19:159-166.

Degaonkar MN, Jayasundar R and Jagannathan NR. Sequential Diffusion-Weighted Magnetic Resonance Imaging Study of Lysophosphatidyl Choline-Induced Experimental Demyelinating Lesion: An Animal Model of Multiple Sclerosis. *J of Magn Reson Imaging* 2002. 16:153–159.

Degaonkar MN, Raghunathan P, Jayasundar R, et al. Determination of relaxation characteristics during preacute stage of lysophosphatidyl choline-induced demyelinating lesion in rat brain: an animal model of multiple sclerosis. *J Magn Reson Imaging* 2005 23:69–73.

Doorduin J, de Vries EFJ, Dierckx RAJO, Klein HC (2008). PET imaging of the peripheral benzodiazepine receptor: monitoring disease progression and therapy response in neurodegenerative disorders. Curr Pharm Des.14(31):3297-315.

Dousset V, Brochet B, Vital A, et al. Lysolecithin-Induced Demyelination in Primates: Preliminary In Vivo Study with MR and Magnetization Transfer 1995 *Am J Neuroradiol* 16:225–231.

Fillip M and Rocca MS. MR Imaging of Multiple Sclerosis. *Radiology* 2011. 259: 659-681.

Gensert JM and Goldman JE. Endogenous Progenitors Remyelinate Demyelinated Axons in the Adult CNS. *Neuron* 1997. 19:197–203.

Hall SM. The effect of injections of lysophosphatidyl choline into white matter of the adult mouse spinal cord. *J Cell Sci* 1972. 10:535-546.

Hall SM and Gregson NA. The in vivo ultrastructural effects of injection of lysophosphatidyl choline into myelinated peripheral nerves fibres of the adult mouse. *J Cell Sci* 1971. 9: 769-789.

Kang H, Lee HY, Lee KS, et al. Imaging-based tumor treatment response evaluation: Review of conventional, new, and emerging concepts. *Korean J Radiol* 2012. 13: 371-390.

Olah M, Amor S, Brouwer N, et al. Identification of a microglia phenotype supportive of remyelination. GLIA 2012. 60:306-321.

Radu CG, Shu CJ, Shelly SM, Phelps ME, Witte ON (2007). Positron emission tomography with computed tomography imaging of neuroinflammation in the experimental encephalomyelitis. Proc Natl Acad Sci U S A; 104:1937-1942.

Rovira A and León A. MR in the diagnosis and monitoring of multiple sclerosis: An overview 2008. Eur J Radiol 67: 409-414.

Stankoff B, et al (2006). Imaging of CNS myelin by positron-emission tomography. PNAS 103: 9304-9309.

Szymanski P, Markowicz M, Janik A, et al. Neuroimaging diagnosis in neurodegenerative diseases. Nucl Med Rev Cent East Eur 2010 13:23-31.

Triarhou LC and Herndon RM. The Effect of Dexamethasone on L-α-Lysophosphatidyl Choline (Lysolecithin)-Induced Demyelination of the Rat Spinal Cord. *Arch Neurol* 1986. 43:121-125.

Waxman SG, Kocsis JD and Nitta KC. Lysophosphatidyl choline-induced focal demyelination in the rabbit corpus callosum. *J Neurol Sci* 1979. 44:45-53.

Woo SK, Lee TS, Kim KM, et al. Anesthesia condition for 18F-FDG imaging of lung metastasis tumors using small animal PET. *Nucl Med Biol* 2008. 35:143–150.

Woodruff RC and Franklin RJM. Demyelination and remyelination of the caudal cerebellar peduncle of adult rats following stereotaxic injections of lysolecithin, ethidium bromide, and complement/anti-galactocerebroside: A comparative study. *GLIA* 1999. 25:216–228.

Wu C, Zhu J, Baeslack J, et al. Longitudinal PET Imaging for Monitoring Myelin Repair in the Spinal Cord. *Ann Neurol* 2013. DOI: 10.1002/ana.23965.

Wu C, Wang C, Popescu DC, et al. A novel PET marker for in vivo quantification of myelination. *Bioorg Med Chem* 2010. 18: 8592–8599.

Wu C, Tian D, Feng Y, et al. A Novel Fluorescent Probe That Is Brain Permeable and Selectively Binds to Myelin. *J Histochem Cytochem* 2006. 54: 997-1004.